Multi-Scaling Bayesian Compressive Sensing Imaging of Dielectric Objects

N. Anselmi, L. Poli, G. Oliveri, and A. Massa

Abstract

In this work, a new Bayesian compressive sensing (*BCS*)-based imaging technique is proposed to exploit additional information besides that on the target *sparsity*. More precisely, an innovative iterative multi-scaling (*IMSA*)-*BCS* scheme is proposed to combine the a-priori knowledge on the class of scatterers and the progressively acquired information on the location and the size of the unknown object. Accordingly the 2D transverse magnetic (*TM*) inverse scattering problem is solved by means of an innovative *IMSA*-based information-driven relevance vector machine (*RVM*) solver. Some numerical results are shown to verify the effectiveness of the proposed imaging technique.

1 Numerical Assessment

1.1 L-shaped Object, $\ell = 1.5\lambda$

Test Case Description

Direct solver:

- Side of the investigation domain: $L = 6.0\lambda$

- Cubic domain divided in $\sqrt{D} \times \sqrt{D}$ cells

- Number of cells for the direct solver: $D = 1600$ (discretization $= \lambda/10$)

Investigation domain:

- Cubic domain divided in $\sqrt{N} \times \sqrt{N}$ cells

- Number of cells for the inversion:
    - First Step IMSA: $N^{(1)} = 100$ (discretization $= \lambda/10$)
    - Following Steps IMSA: $N^{(i)}$ not fixed, defined according to the estimated RoI $\mathcal{D}^{(i)}$

Measurement domain:

- Total number of measurements: $M = 60$

- Measurement points placed on circles of radius $\rho = 4.5\lambda$

Sources:

- Plane waves

- Number of views: $V = 60$; $\theta_{inc}^v = 0° + (v-1) \times (360/V)$

- Amplitude: $A = 1.0$

- Frequency: $F = 300$ MHz ($\lambda = 1$)

Background:

- $\varepsilon_r = 1.0$

- $\sigma = 0$ [S/m]

Scatterer

- L-shaped object, $\ell = 1.5\lambda$

- $\varepsilon_r \in \{1.01, 1.02, 1.04, 1.05, 1.06, 1.08, 1.10, 1.15, 1.20\}$
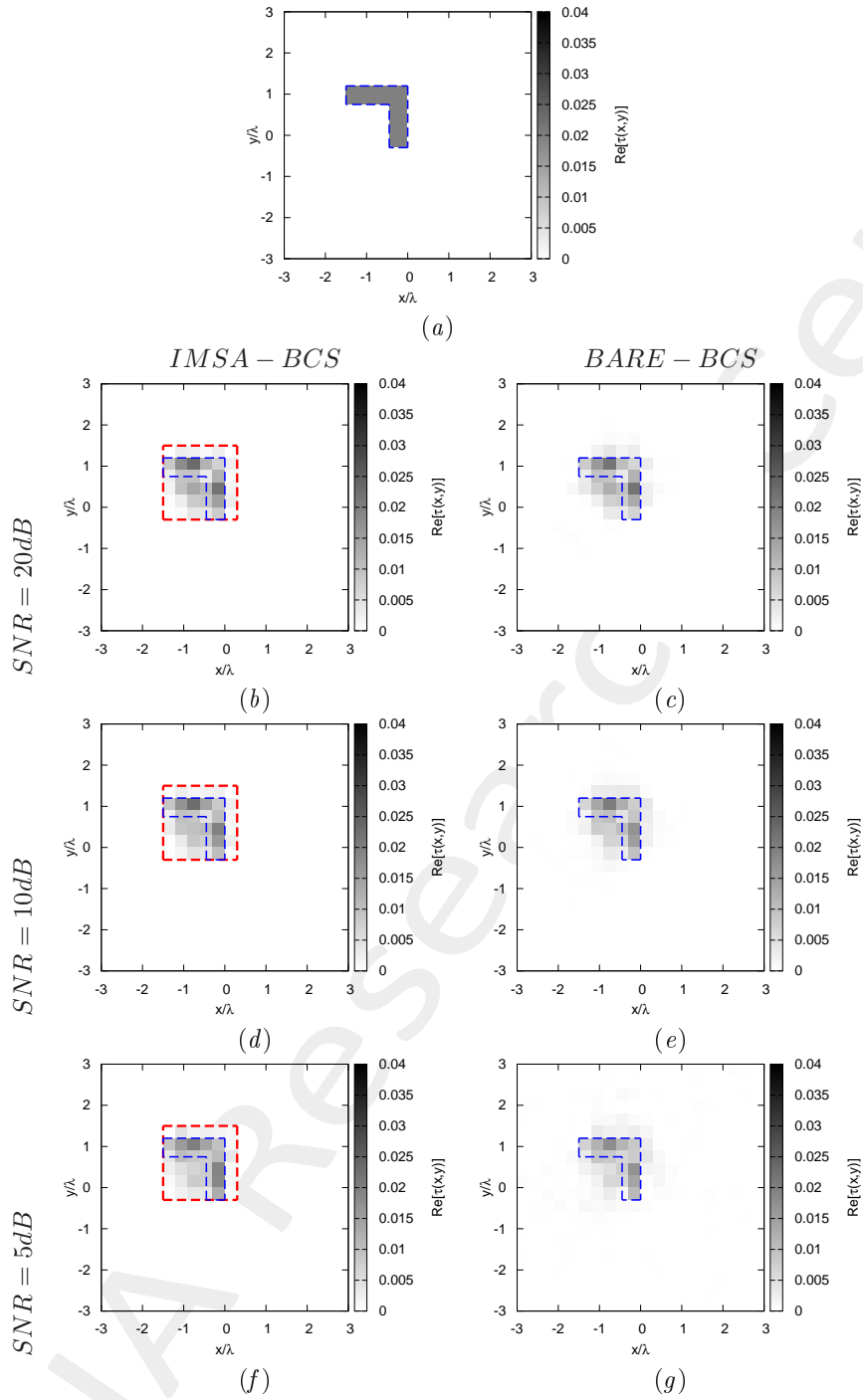
- $\sigma = 0$ [S/m]

Figure 1: *L-shaped Object, $\ell = 1.5\lambda$, IMSA-BCS vs. BARE-BCS, $\ell = 1.5\lambda$, $\tau = 0.02$* - (*a*) Actual profile, (*b*)(*d*)(*f*) *IMSA − BCS* and *BARE − BCS* reconstructed profiles for (*b*)(*c*) *SNR* = 20 [dB], (*d*)(*e*) *SNR* = 10 [dB] and (*f*)(*g*) *SNR* = 5 [dB].

	SNR = 50dB	
	$IMSA - BCS$	$BARE - BCS$
ξ_{tot}	5.64×10^{-4}	5.15×10^{-4}
ξ_{int}	1.04×10^{-2}	9.08×10^{-3}
ξ_{ext}	2.39×10^{-4}	2.32×10^{-4}
	SNR = 20dB	
	$IMSA - BCS$	$BARE - BCS$
ξ_{tot}	5.72×10^{-4}	5.26×10^{-4}
ξ_{int}	1.04×10^{-2}	9.26×10^{-3}
ξ_{ext}	2.47×10^{-4}	2.37×10^{-4}
	SNR = 10dB	
	$IMSA - BCS$	$BARE - BCS$
ξ_{tot}	5.42×10^{-4}	5.36×10^{-4}
ξ_{int}	1.01×10^{-2}	9.17×10^{-3}
ξ_{ext}	2.24×10^{-4}	2.49×10^{-4}
	SNR = 5dB	
	$IMSA - BCS$	$BARE - BCS$
ξ_{tot}	4.34×10^{-4}	6.03×10^{-4}
ξ_{int}	7.44×10^{-3}	9.57×10^{-3}
ξ_{ext}	2.01×10^{-4}	2.85×10^{-4}

Table I: *L-shaped Object, $\ell = 1.5\lambda$, IMSA-BCS vs. BARE-BCS, $\tau = 0.02$* - Reconstruction errors: total (ξ_{tot}), internal (ξ_{int}) and external (ξ_{ext}) errors.
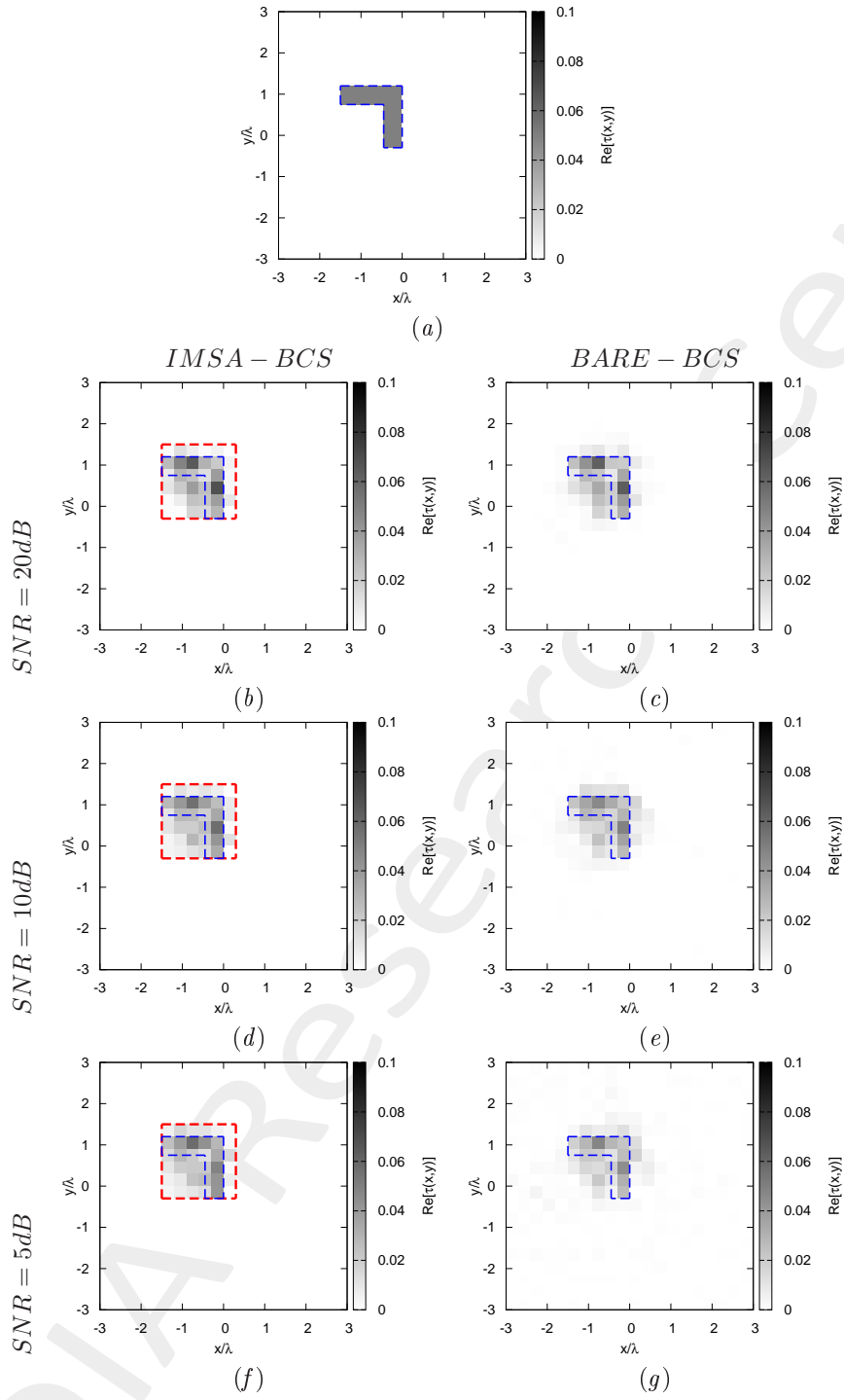
Figure 2: *L-shaped Object, $\ell = 1.5\lambda$, IMSA-BCS vs. BARE-BCS, $\tau = 0.05$* - (a) Actual profile, $(b)(d)(f)$ $IMSA - BCS$ and $BARE - BCS$ reconstructed profiles for $(b)(c)$ $SNR = 20$ [dB], $(d)(e)$ $SNR = 10$ [dB] and $(f)(g)$ $SNR = 5$ [dB].

	$SNR = 50dB$	
	$IMSA - BCS$	$BARE - BCS$
ξ_{tot}	1.23×10^{-3}	1.31×10^{-3}
ξ_{int}	1.99×10^{-2}	2.00×10^{-2}
ξ_{ext}	6.12×10^{-4}	6.78×10^{-4}
	$SNR = 20dB$	
	$IMSA - BCS$	$BARE - BCS$
ξ_{tot}	1.23×10^{-3}	1.39×10^{-3}
ξ_{int}	1.98×10^{-2}	2.14×10^{-2}
ξ_{ext}	6.17×10^{-4}	7.21×10^{-4}
	$SNR = 10dB$	
	$IMSA - BCS$	$BARE - BCS$
ξ_{tot}	1.19×10^{-3}	1.57×10^{-3}
ξ_{int}	1.74×10^{-2}	2.01×10^{-2}
ξ_{ext}	6.50×10^{-4}	8.84×10^{-4}
	$SNR = 5dB$	
	$IMSA - BCS$	$BARE - BCS$
ξ_{tot}	1.19×10^{-3}	1.98×10^{-3}
ξ_{int}	1.66×10^{-2}	2.31×10^{-2}
ξ_{ext}	6.73×10^{-4}	1.09×10^{-3}

Table II: *L-shaped Object*, $\ell = 1.5\lambda$, *IMSA-BCS vs. BARE-BCS*, $\tau = 0.05$ - Reconstruction errors: total (ξ_{tot}), internal (ξ_{int}) and external (ξ_{ext}) errors.

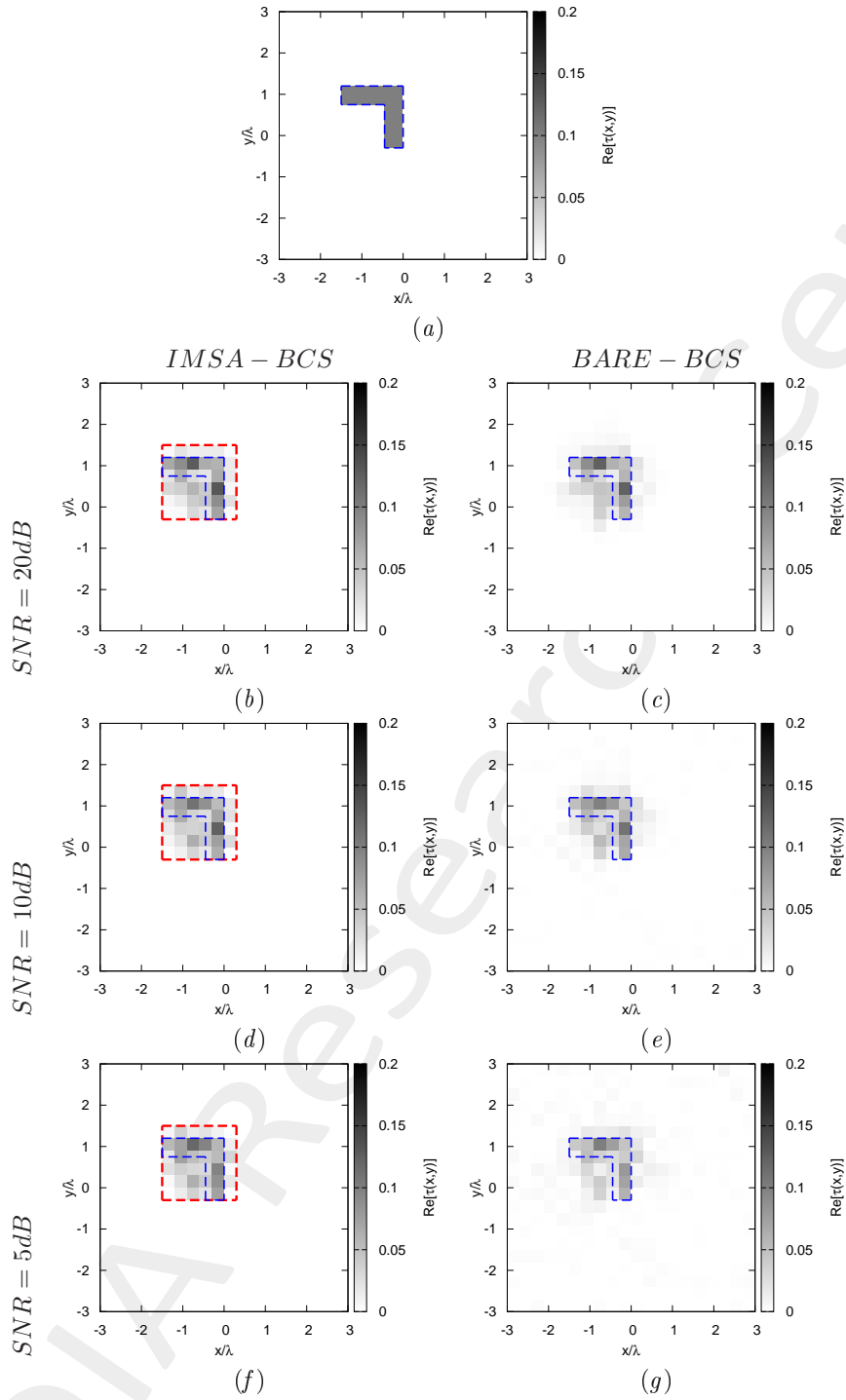### 1.1.3 L-shaped Object, $\ell = 1.5\lambda$, $\tau = 0.10$ - IMSA-BCS vs. BARE-BCS reconstructed profiles

Figure 3: *L-shaped Object, $\ell = 1.5\lambda$, IMSA-BCS vs. BARE-BCS, $\tau = 0.10$ -* (a) Actual profile, $(b)(d)(f)$ $IMSA - BCS$ and $BARE - BCS$ reconstructed profiles for $(b)(c)$ $SNR = 20$ [dB], $(d)(e)$ $SNR = 10$ [dB] and $(f)(g)$ $SNR = 5$ [dB].

	$SNR = 50dB$	
	$IMSA - BCS$	$BARE - BCS$
ξ_{tot}	2.36×10^{-3}	2.63×10^{-3}
ξ_{int}	3.50×10^{-2}	3.67×10^{-2}
ξ_{ext}	1.21×10^{-3}	1.40×10^{-3}
	$SNR = 20dB$	
	$IMSA - BCS$	$BARE - BCS$
ξ_{tot}	2.42×10^{-3}	2.88×10^{-3}
ξ_{int}	3.57×10^{-2}	4.02×10^{-2}
ξ_{ext}	1.25×10^{-3}	1.52×10^{-3}
	$SNR = 10dB$	
	$IMSA - BCS$	$BARE - BCS$
ξ_{tot}	2.55×10^{-3}	3.25×10^{-3}
ξ_{int}	3.55×10^{-2}	3.71×10^{-2}
ξ_{ext}	1.39×10^{-3}	1.86×10^{-3}
	$SNR = 5dB$	
	$IMSA - BCS$	$BARE - BCS$
ξ_{tot}	2.47×10^{-3}	4.29×10^{-3}
ξ_{int}	3.22×10^{-2}	4.33×10^{-2}
ξ_{ext}	1.36×10^{-3}	2.44×10^{-3}

Table III: *L-shaped Object*, $\ell = 1.5\lambda$, *IMSA-BCS vs. BARE-BCS*, $\tau = 0.10$ - Reconstruction errors: total (ξ_{tot}), internal (ξ_{int}) and external (ξ_{ext}) errors.
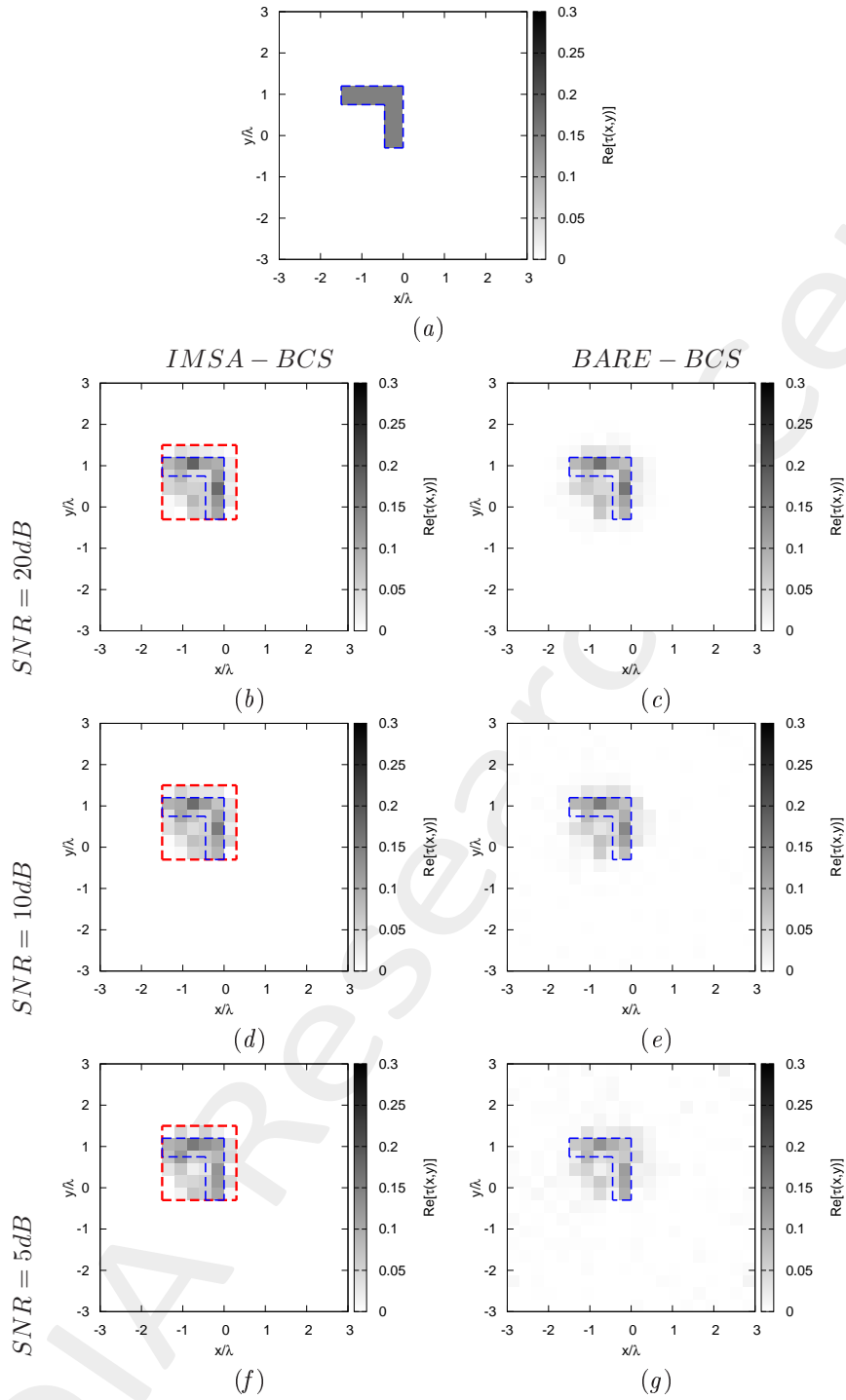
Figure 4: *L-shaped Object, $\ell = 1.5\lambda$, IMSA-BCS vs. BARE-BCS, $\tau = 0.15$* - (a) Actual profile, $(b)(d)(f)$ $IMSA - BCS$ and $BARE - BCS$ reconstructed profiles for $(b)(c)$ $SNR = 20$ [dB], $(d)(e)$ $SNR = 10$ [dB] and $(f)(g)$ $SNR = 5$ [dB].

	$SNR = 50dB$	
	$IMSA - BCS$	$BARE - BCS$
ξ_{tot}	3.48×10^{-3}	4.04×10^{-3}
ξ_{int}	4.62×10^{-2}	5.20×10^{-2}
ξ_{ext}	1.79×10^{-3}	2.17×10^{-3}
	$SNR = 20dB$	
	$IMSA - BCS$	$BARE - BCS$
ξ_{tot}	3.69×10^{-3}	4.38×10^{-3}
ξ_{int}	4.97×10^{-2}	5.50×10^{-2}
ξ_{ext}	1.92×10^{-3}	2.39×10^{-3}
	$SNR = 10dB$	
	$IMSA - BCS$	$BARE - BCS$
ξ_{tot}	3.87×10^{-3}	5.28×10^{-3}
ξ_{int}	5.03×10^{-2}	5.53×10^{-2}
ξ_{ext}	2.10×10^{-3}	3.00×10^{-3}
	$SNR = 5dB$	
	$IMSA - BCS$	$BARE - BCS$
ξ_{tot}	3.85×10^{-3}	6.99×10^{-3}
ξ_{int}	4.50×10^{-2}	6.41×10^{-2}
ξ_{ext}	2.06×10^{-3}	3.90×10^{-3}

Table IV: *L-shaped Object*, $\ell = 1.5\lambda$, *IMSA-BCS vs. BARE-BCS*, $\tau = 0.15$ - Reconstruction errors: total (ξ_{tot}), internal (ξ_{int}) and external (ξ_{ext}) errors.

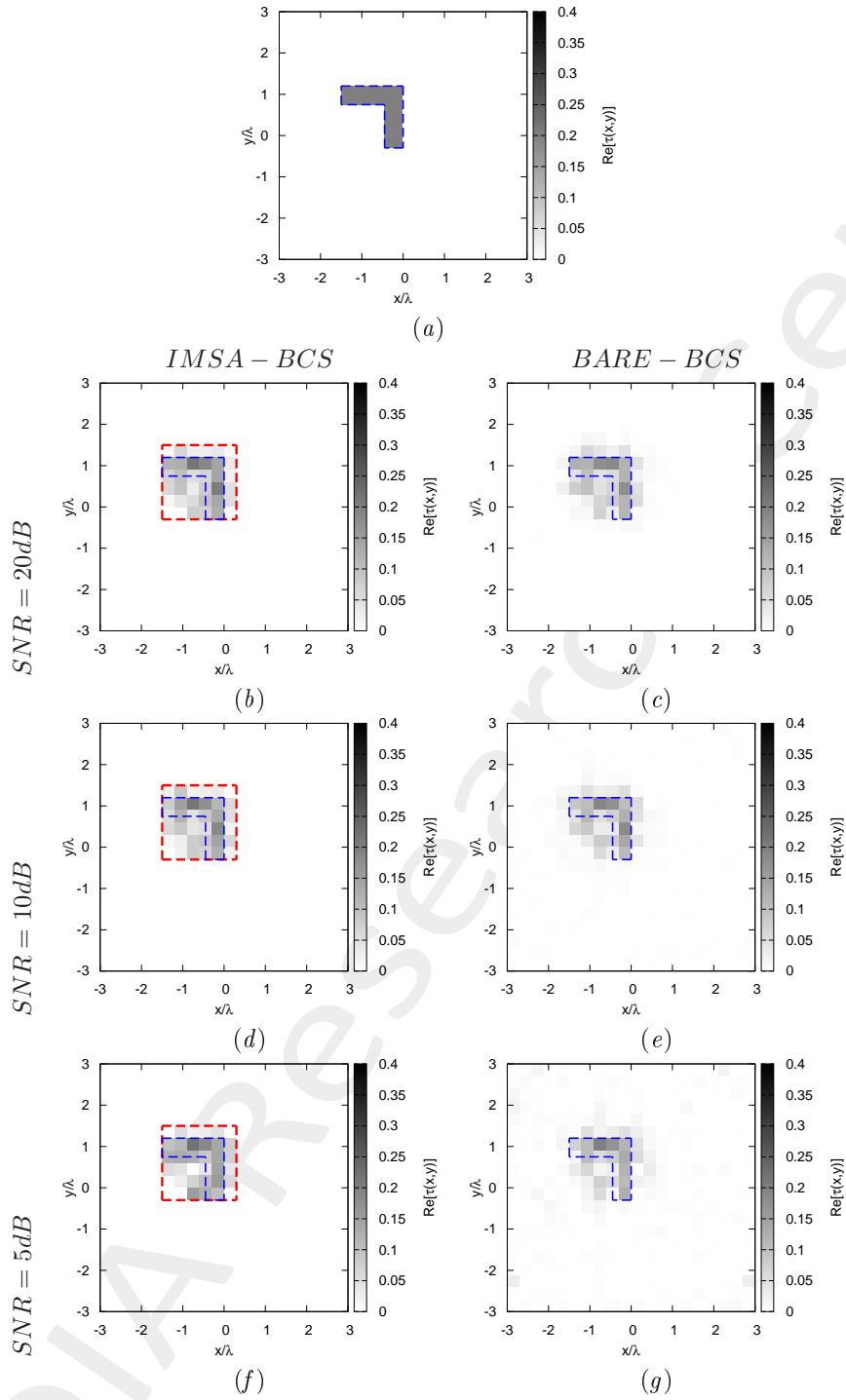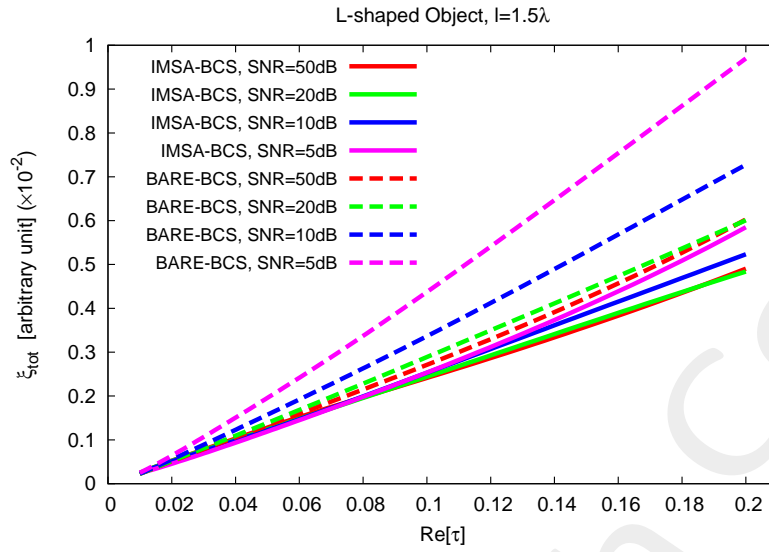### 1.1.5   L-shaped Object, $\ell = 1.5\lambda$, $\tau = 0.20$ - IMSA-BCS vs. BARE-BCS reconstructed profiles

Figure 5: *L-shaped Object*, $\ell = 1.5\lambda$, *IMSA-BCS vs. BARE-BCS*, $\ell = 1.5\lambda$, $\tau = 0.20$ - (a) Actual profile, $(b)(d)(f)$ $IMSA-BCS$ and $BARE-BCS$ reconstructed profiles for $(b)(c)$ $SNR = 20$ [dB], $(d)(e)$ $SNR = 10$ [dB] and $(f)(g)$ $SNR = 5$ [dB].
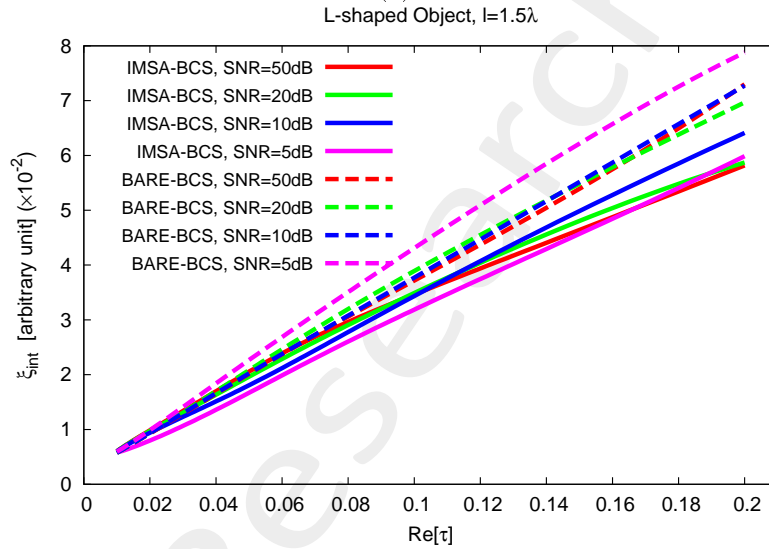
	SNR = 50dB	
	$IMSA - BCS$	$BARE - BCS$
ξ_{tot}	4.90×10^{-3}	6.02×10^{-3}
ξ_{int}	5.81×10^{-2}	7.29×10^{-2}
ξ_{ext}	2.58×10^{-3}	3.23×10^{-3}
	SNR = 20dB	
	$IMSA - BCS$	$BARE - BCS$
ξ_{tot}	4.83×10^{-3}	6.00×10^{-3}
ξ_{int}	5.87×10^{-2}	6.96×10^{-2}
ξ_{ext}	2.51×10^{-3}	3.23×10^{-3}
	SNR = 10dB	
	$IMSA - BCS$	$BARE - BCS$
ξ_{tot}	5.23×10^{-3}	7.27×10^{-3}
ξ_{int}	6.41×10^{-2}	7.27×10^{-2}
ξ_{ext}	2.75×10^{-3}	3.98×10^{-3}
	SNR = 5dB	
	$IMSA - BCS$	$BARE - BCS$
ξ_{tot}	5.85×10^{-3}	9.69×10^{-3}
ξ_{int}	5.98×10^{-2}	7.87×10^{-2}
ξ_{ext}	3.09×10^{-3}	5.25×10^{-3}

Table V: *L-shaped Object*, $\ell = 1.5\lambda$, *IMSA-BCS vs. BARE-BCS*, $\tau = 0.20$ - Reconstruction errors: total (ξ_{tot}), internal (ξ_{int}) and external (ξ_{ext}) errors.
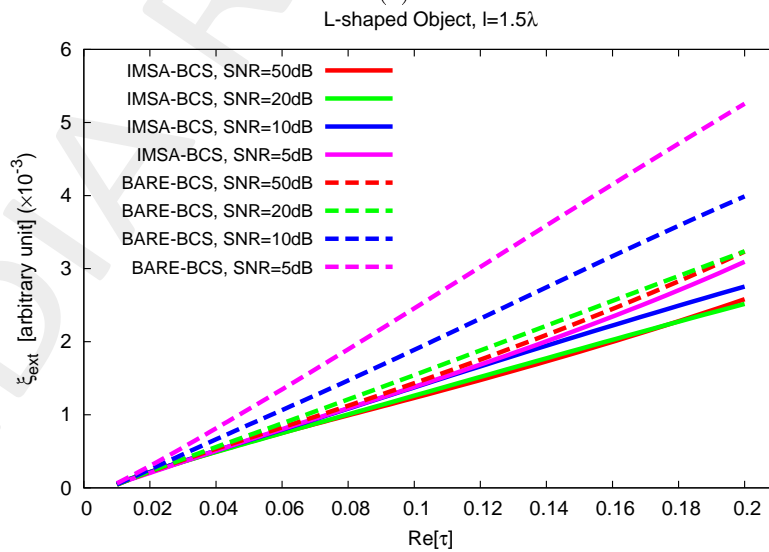
Figure 6: *L-shaped Object, $\ell = 1.5\lambda$* - Reconstruction errors vs. τ: (a) total error, (b) internal error and (c) external error.

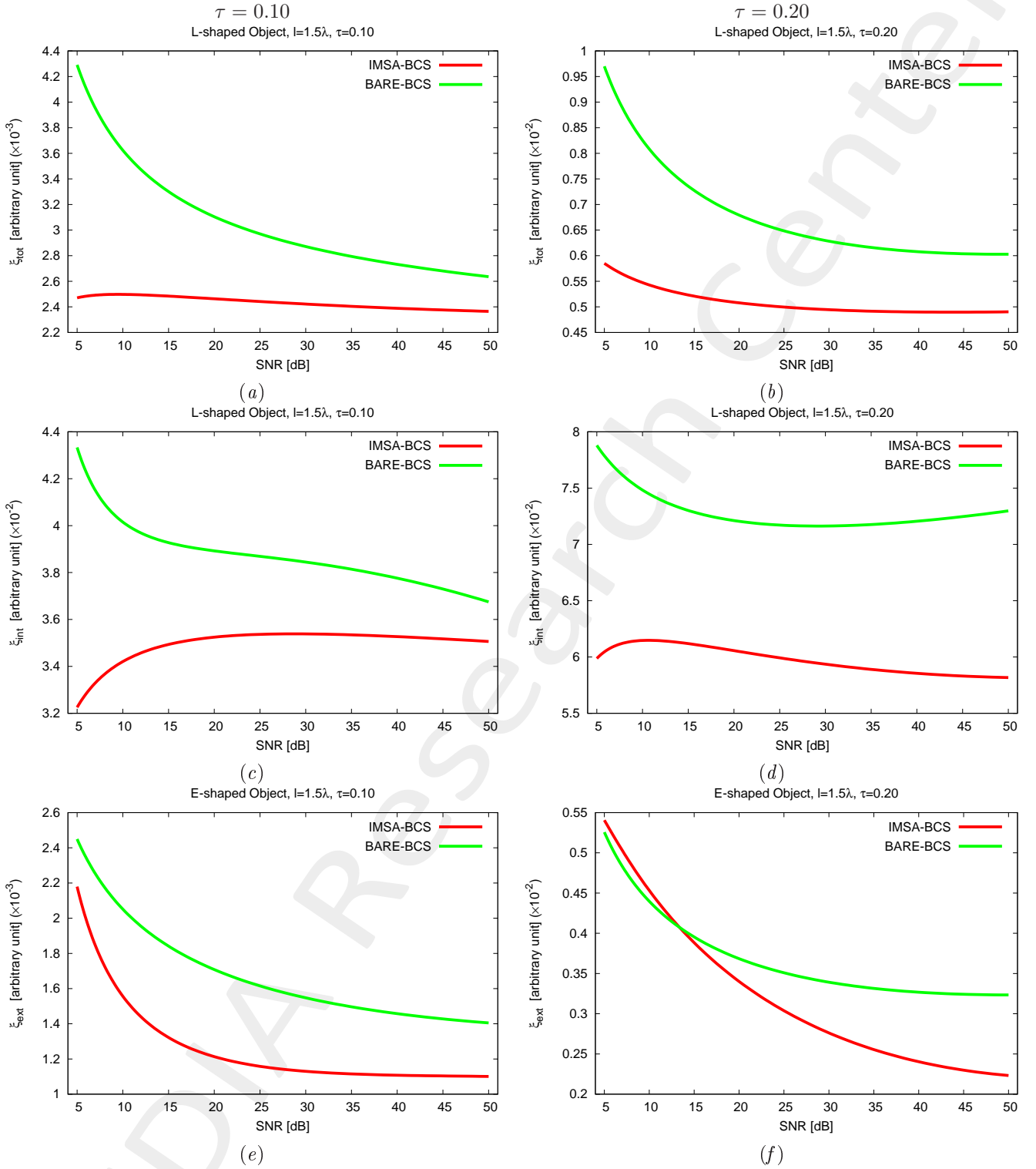$\tau = 0.10$ $\qquad\qquad\qquad\qquad\qquad\qquad\qquad$ $\tau = 0.20$

Figure 7: *L-shaped Object*, $\ell = 1.5\lambda$ - Reconstruction errors vs. SNR: $(a)(b)$ total error, $(c)(d)$ internal error and $(e)(f)$ external error for $(a)(c)(e)$ $\tau = 0.10$ and $(b)(d)(f)$ $\tau = 0.20$.

1.2 Inhomogeneous Square Object, $\ell = 1.5\lambda$

Test Case Description

Direct solver:

- Side of the investigation domain: $L = 6.0\lambda$

- Cubic domain divided in $\sqrt{D} \times \sqrt{D}$ cells

- Number of cells for the direct solver: $D = 1600$ (discretization $= \lambda/10$)

Investigation domain:

- Cubic domain divided in $\sqrt{N} \times \sqrt{N}$ cells

- Number of cells for the inversion:
  - First Step IMSA: $N^{(1)} = 100$ (discretization $= \lambda/10$)
  - Following Steps IMSA: $N^{(i)}$ not fixed, defined according to the estimated RoI $\mathcal{D}^{(i)}$

Measurement domain:

- Total number of measurements: $M = 60$

- Measurement points placed on circles of radius $\rho = 4.5\lambda$

Sources:

- Plane waves

- Number of views: $V = 60$; $\theta_{inc}^v = 0° + (v-1) \times (360/V)$

- Amplitude: $A = 1.0$

- Frequency: $F = 300$ MHz ($\lambda = 1$)

Background:

- $\varepsilon_r = 1.0$

- $\sigma = 0$ [S/m]

Scatterer

- Inhomogeneous square object, $\ell = 1.5\lambda$

- $\varepsilon_r^{(1)} \in \{1.02, 1.04, 1.06, 1.08, 1.10, 1.12, 1.14, 1.16, 1.20\}$ (internal circle)
  $\varepsilon_r^{(2)} = \frac{\varepsilon_r^{(1)}}{2}$ (central circle)
  $\varepsilon_r^{(3)} = \frac{\varepsilon_r^{(1)}}{4}$ (external circle)

- $\sigma = 0$ [S/m]

1.2.1 Inhomogeneous Square Object, $\ell = 1.5\lambda$, $\tau^{(1)} = 0.02$ - IMSA-BCS vs. BARE-BCS reconstructed profiles
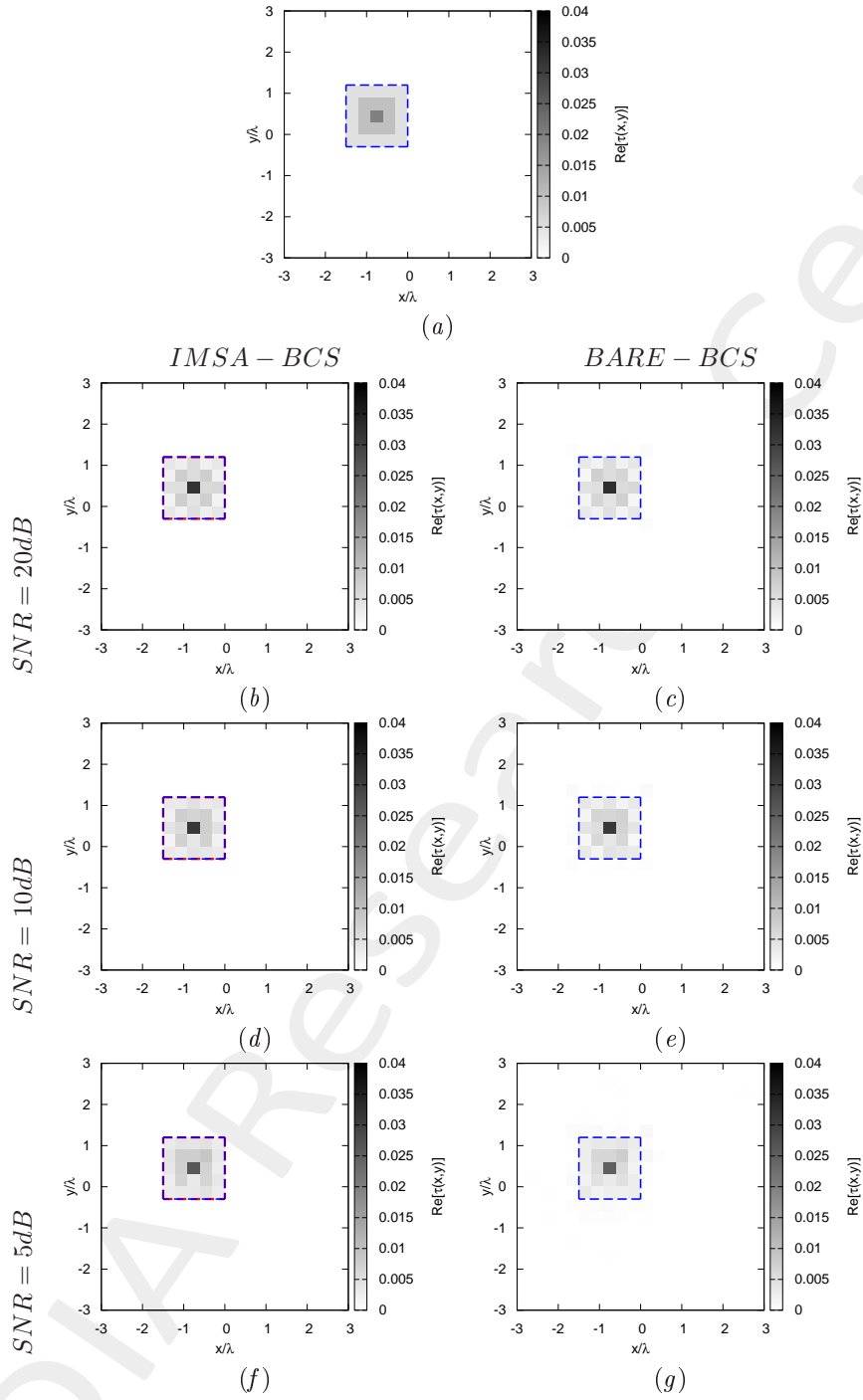

Figure 8: *Inhomogeneous Square Object, $\ell = 1.5\lambda$, $\tau^{(1)} = 0.02$ - IMSA-BCS vs. BARE-BCS* - (a) Actual profile, (b)(d)(f) *IMSA* − *BCS* and *BARE* − *BCS* reconstructed profiles for (b)(c) $SNR = 20$ [dB], (d)(e) $SNR = 10$ [dB] and (f)(g) $SNR = 5$ [dB].

	SNR = 50dB	
	$IMSA - BCS$	$BARE - BCS$
ξ_{tot}	1.74×10^{-4}	1.93×10^{-4}
ξ_{int}	2.78×10^{-3}	2.95×10^{-3}
ξ_{ext}	0.00×10^{-1}	9.06×10^{-6}
	SNR = 20dB	
	$IMSA - BCS$	$BARE - BCS$
ξ_{tot}	1.72×10^{-4}	1.99×10^{-4}
ξ_{int}	2.75×10^{-3}	3.00×10^{-3}
ξ_{ext}	0.00×10^{-1}	1.18×10^{-5}
	SNR = 10dB	
	$IMSA - BCS$	$BARE - BCS$
ξ_{tot}	1.58×10^{-4}	2.03×10^{-4}
ξ_{int}	2.53×10^{-3}	2.90×10^{-3}
ξ_{ext}	0.00×10^{-1}	2.29×10^{-5}
	SNR = 5dB	
	$IMSA - BCS$	$BARE - BCS$
ξ_{tot}	1.30×10^{-4}	2.42×10^{-4}
ξ_{int}	2.09×10^{-3}	2.91×10^{-3}
ξ_{ext}	0.00×10^{-1}	6.12×10^{-5}

Table VI: *Inhomogeneous Square Object*, $\ell = 1.5\lambda$, $\tau^{(1)} = 0.02$ - *IMSA-BCS vs. BARE-BCS* - Reconstruction errors: total (ξ_{tot}), internal (ξ_{int}) and external (ξ_{ext}) errors.

1.2.2 Inhomogeneous Square Object, $\ell = 1.5\lambda$, $\tau^{(1)} = 0.04$ - IMSA-BCS vs. BARE-BCS reconstructed profiles
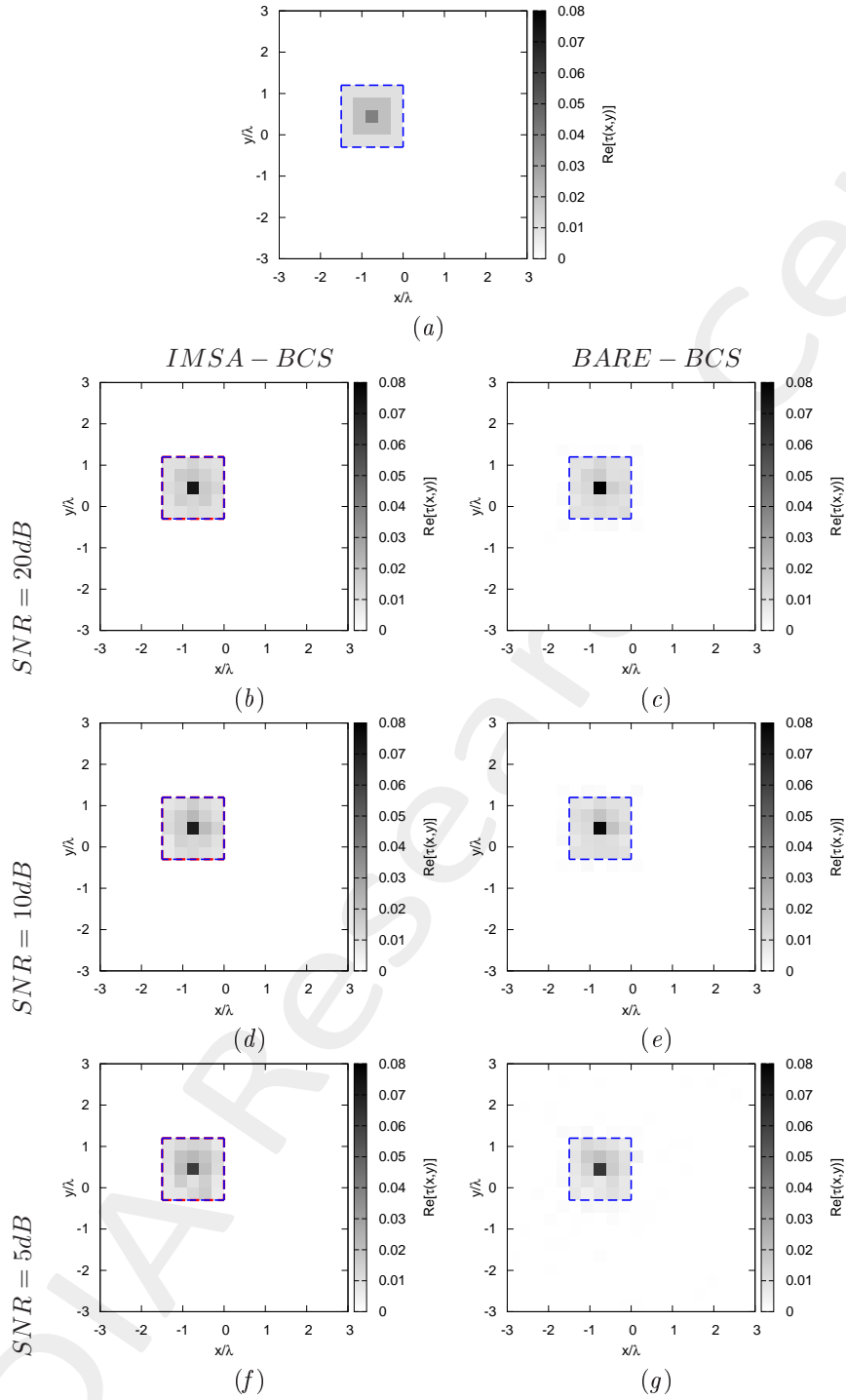

Figure 9: *Inhomogeneous Square Object, $\ell = 1.5\lambda$, $\tau^{(1)} = 0.04$ - IMSA-BCS vs. BARE-BCS* - (a) Actual profile, (b)(d)(f) *IMSA − BCS* and *BARE − BCS* reconstructed profiles for (b)(c) $SNR = 20$ [dB], (d)(e) $SNR = 10$ [dB] and (f)(g) $SNR = 5$ [dB].

	SNR = 50dB	
	$IMSA - BCS$	$BARE - BCS$
ξ_{tot}	2.14×10^{-4}	3.25×10^{-4}
ξ_{int}	3.42×10^{-3}	4.44×10^{-3}
ξ_{ext}	0.00×10^{-1}	5.11×10^{-5}
	SNR = 20dB	
	$IMSA - BCS$	$BARE - BCS$
ξ_{tot}	2.13×10^{-4}	3.27×10^{-4}
ξ_{int}	3.41×10^{-3}	4.44×10^{-3}
ξ_{ext}	0.00×10^{-1}	5.28×10^{-5}
	SNR = 10dB	
	$IMSA - BCS$	$BARE - BCS$
ξ_{tot}	2.33×10^{-4}	3.34×10^{-4}
ξ_{int}	3.72×10^{-3}	4.14×10^{-3}
ξ_{ext}	0.00×10^{-1}	7.19×10^{-5}
	SNR = 5dB	
	$IMSA - BCS$	$BARE - BCS$
ξ_{tot}	2.13×10^{-4}	5.09×10^{-4}
ξ_{int}	3.36×10^{-3}	4.20×10^{-3}
ξ_{ext}	0.00×10^{-1}	2.07×10^{-4}

Table VII: *Inhomogeneous Square Object*, $\ell = 1.5\lambda$, $\tau^{(1)} = 0.04$ - *IMSA-BCS vs. BARE-BCS* - Reconstruction errors: total (ξ_{tot}), internal (ξ_{int}) and external (ξ_{ext}) errors.

More information on the topics of this document can be found in the following list of references.

References

[1] M. Salucci, G. Oliveri, and A. Massa, "GPR prospecting through an inverse scattering frequency-hopping multi-focusing approach," *IEEE Trans. Geosci. Remote Sens.*, vol. 53, no. 12, pp. 6573-6592, Dec. 2015.

[2] M. Salucci, L. Poli, N. Anselmi, and A. Massa, "Multifrequency Particle Swarm Optimization for enhanced multi-tiresolution GPR microwave imaging," *IEEE Trans. Geosci. Remote Sens.*, vol. 55, no. 3, pp. 1305-1317, Mar. 2017.

[3] M. Salucci, L. Poli, and A. Massa, "Advanced multi-frequency GPR data processing for non-linear deterministic imaging," *Signal Processing*, vol. 132, pp. 306-318, Mar. 2017.

[4] N. Anselmi, G. Oliveri, M. Salucci, and A. Massa, "Wavelet-based compressive imaging of sparse targets," *IEEE Trans. Antennas Propag.*, vol. 63, no. 11, pp. 4889-4900, Nov. 2015.

[5] G. Oliveri, M. Salucci, N. Anselmi, and A. Massa, "Compressive sensing as applied to inverse problems for imaging: theory, applications, current trends, and open challenges," *IEEE Antennas Propag. Mag.*, vol. 59, no. 5, pp. 34-46, Oct. 2017.

[6] A. Massa, P. Rocca, and G. Oliveri, "Compressive sensing in electromagnetics - A review," *IEEE Antennas Propag. Mag.*, pp. 224-238, vol. 57, no. 1, Feb. 2015.

[7] N. Anselmi, L. Poli, G. Oliveri, and A. Massa, "Iterative multi-resolution bayesian CS for microwave imaging," *IEEE Trans. Antennas Propag.*, vol. 66, no. 7, pp. 3665-3677, Jul. 2018.

[8] N. Anselmi, G. Oliveri, M. A. Hannan, M. Salucci, and A. Massa, "Color compressive sensing imaging of arbitrary-shaped scatterers," *IEEE Trans. Microw. Theory Techn.*, vol. 65, no. 6, pp. 1986-1999, Jun. 2017.

[9] G. Oliveri, N. Anselmi, and A. Massa, "Compressive sensing imaging of non-sparse 2D scatterers by a total-variation approach within the Born approximation," *IEEE Trans. Antennas Propag.*, vol. 62, no. 10, pp. 5157-5170, Oct. 2014.

[10] L. Poli, G. Oliveri, and A. Massa, "Imaging sparse metallic cylinders through a local shape function Bayesian compressive sensing approach," *J. Opt. Soc. Am. A*, vol. 30, no. 6, pp. 1261-1272, 2013.

[11] L. Poli, G. Oliveri, F. Viani, and A. Massa, "MT-BCS-based microwave imaging approach through minimum-norm current expansion," *IEEE Trans. Antennas Propag.*, vol. 61, no. 9, pp. 4722-4732, Sep. 2013.

[12] F. Viani, L. Poli, G. Oliveri, F. Robol, and A. Massa, "Sparse scatterers imaging through approximated multitask compressive sensing strategies," *Microwave Opt. Technol. Lett.*, vol. 55, no. 7, pp. 1553-1558, Jul. 2013.

[13] L. Poli, G. Oliveri, P. Rocca, and A. Massa, "Bayesian compressive sensing approaches for the reconstruction of two-dimensional sparse scatterers under TE illumination," *IEEE Trans. Geosci. Remote Sens.*, vol. 51, no. 5, pp. 2920-2936, May 2013.

[14] L. Poli, G. Oliveri, and A. Massa,"Microwave imaging within the first-order Born approximation by means of the contrast-field Bayesian compressive sensing," *IEEE Trans. Antennas Propag.*, vol. 60, no. 6, pp. 2865-2879, Jun. 2012.

[15] G. Oliveri, L. Poli, P. Rocca, and A. Massa,"Bayesian compressive optical imaging within the Rytov approximation," *Optics Letters*, vol. 37, no. 10, pp. 1760-1762, 2012.

[16] G. Oliveri, P. Rocca, and A. Massa,"A Bayesian compressive sampling-based inversion for imaging sparse scatterers," *IEEE Trans. Geosci. Remote Sens.*, vol. 49, no. 10, pp. 3993-4006, Oct. 2011.

[17] G. Oliveri, M. Salucci, and N. Anselmi,"Tomographic imaging of sparse low-contrast targets in harsh environments through matrix completion," *IEEE Trans. Microw. Theory Tech.*, vol. 66, no. 6, pp. 2714-2730, Jun. 2018.

[18] M. Salucci, A. Gelmini, L. Poli, G. Oliveri, and A. Massa,"Progressive compressive sensing for exploiting frequency-diversity in GPR imaging," *J. Electromagn. Waves Appl.*, vol. 32, no. 9, pp. 1164- 1193, 2018.